Materials Research Proceedings 28 (2023) 477-486 https://doi.org/10.21741/9781644902479-52

Experimental analysis and modeling of the recrystallization behaviour of a AA6060 extruded profile

NEGOZIO Marco[1,a *], DONATI Lorenzo[1,b], PELACCIA Riccardo[2,c], REGGIANI Barbara[2,d] and DI DONATO Sara[1,e]

[1]DIN Department of Industrial Engineering – University of Bologna, Viale Risorgimento 2, 40136, Bologna, Italy

[2]DISMI Department of Sciences and Methods for Engineering, University of Modena and Reggio Emilia, Via Amendola 2, 42122, Reggio Emilia, Italy

[a]marco.negozio2@unibo.it, [b]l.donati@unibo.it, [c]riccardo.pelaccia@unimore.it, [d]barbara.reggiani@unimore.it, [e]sara.didonato2@unibo.it

Keywords: Recrystallization, Aluminum Alloy, Extrusion, FEM, Microstructure, 6XXX

Abstract. The microstructure of Al-Mg-Si alloys is gaining nowadays an increasing industrial interest because it influences the strength, crash, corrosion and esthetic properties of the extruded profiles. In order to investigate and predict the recrystallization behaviour in the extrusion of 6XXX aluminum alloys, experimental and numerical activities are still needed. In this work, the extrusion of an industrial-scale AA6060 aluminum alloy hollow profile was carried out. An innovative recrystallization model was developed and optimized by comparing the microstructural data experimentally acquired with the outputs of the simulation performed using the Finite Element commercial code Qform Extrusion. A good correlation between numerical prediction and experimental data was found, thus proving the reliability of the proposed AA6060 recrystallization model.

Introduction

The microstructure of 6XXX aluminum alloy extruded profiles is of primary interest for extrusion companies since it affects the product performances [1,2]. To date, the relationship between process parameters and grain structure evolution is not fully understood due to the high number of factors that affects the final microstructure of the profile. For this reason, the scientific community is pooling efforts to investigate the recrystallization of aluminum alloys during the extrusion process. Moreover, in order to control the final microstructure at a die design stage without performing expensive experimental trial and errors, it is mandatory the development of reliable models for the recrystallization prediction to be implemented into FE (Finite Element) codes.

In Fig. 1, a typical microstructural evolution during the extrusion of 6XXX aluminum alloys is shown. Two different types of structures can be detected. In the fibrous structure (Fig. 1b,d), grains are deeply elongated and they are characterized by a length (the dimension along the extrusion direction) several times greater than the width and thickness. Instead, in the recrystallized structure (Fig. 1c,e), grains have a spherical equiaxed shape (Fig. 1a) so that they can be characterized by a single average grain diameter. The fully recrystallized state is always detectable in the billet material as consequence of the casting phase and further homogenization process. Immediately after the die exit, the profile always shows a fibrous microstructure (immediate profile quenching) due to the strain field applied during the extrusion process. If the profile is not immediately quenched and its temperature remains higher than the alloy recrystallization temperature for a sufficient amount of time, the structure may recrystallize (fully or partially Fig. 1c,e). If the energy stored in the material during the deformation process is lower than a certain critical level, the microstructure of the profile still remains fibrous (Fig. 1d).

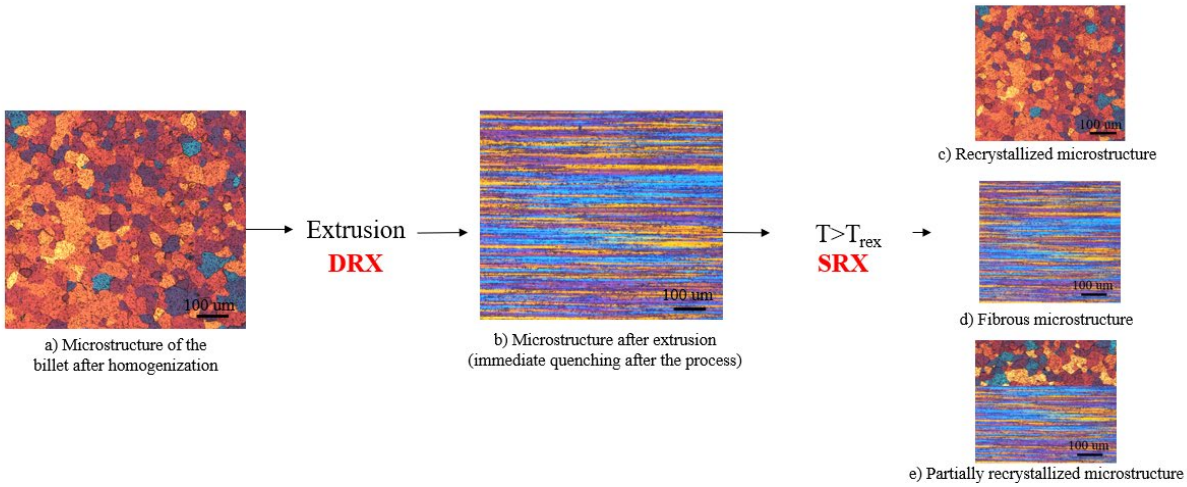

Fig. 1. schematization of the microstructure evolution during the extrusion process of a 6XXX aluminum alloy.

During and after the extrusion of 6XXX aluminum alloys, two main recrystallization mechanisms can be distinguished: the first, called dynamic recrystallization (DRX), occurs while the material is deforming [3]. This phenomenon is related to the material strain field and involves, for low stacking fault materials (LSFE), nucleation and grain growth or, for high stacking fault materials (HSFE as aluminum alloys), other different behaviours that are still under debate in the research community.

The second main recrystallization mechanism is the static recrystallization (SRX), which occurs after the hot deformation and causes the rearrangement of the microstructure through nucleation and growth [4]. Several studies have been made to investigate the SRX in the hot deformation processes of aluminum alloys also using finite element model simulations [5-7]. However, many of these works were performed using laboratory-scale or simple-profile extrusions as experimental campaigns. Moreover, none of the investigated models has been extensively tested on extrusions of industrial-scale cases or on complex geometry profiles, thus limiting the strain and strain rate fields for the modeling validation.

In this work, an industrial-scale extrusion of AA6060 aluminum alloy hollow profile was investigated. Numerical activities involving Finite Element (FE) simulation of the extrusion were performed with the commercial Qform Extrusion code. Moreover, an innovative recrystallization model was developed, comparing the achieved results with the microstructural data experimentally collected for the industrial-scale profile. The final aim of this work was to propose a reliable model able to accurately predict the microstructural behaviour in the hot extrusion of AA6060 aluminum alloy profiles.

Experimental Procedure

The geometry of the profile under investigation is reported in Fig. 2. It was produced by the Profilati SpA plant of Medicina (Italy). The production batch involved the extrusion of 17 billets and the data about profile exit temperature and extrusion load were acquired during the whole process and used to validate the numerical simulation results. The analyzed sample comes from the extrusion of the seventh billet in order to have steady-state conditions in the tool-die set.

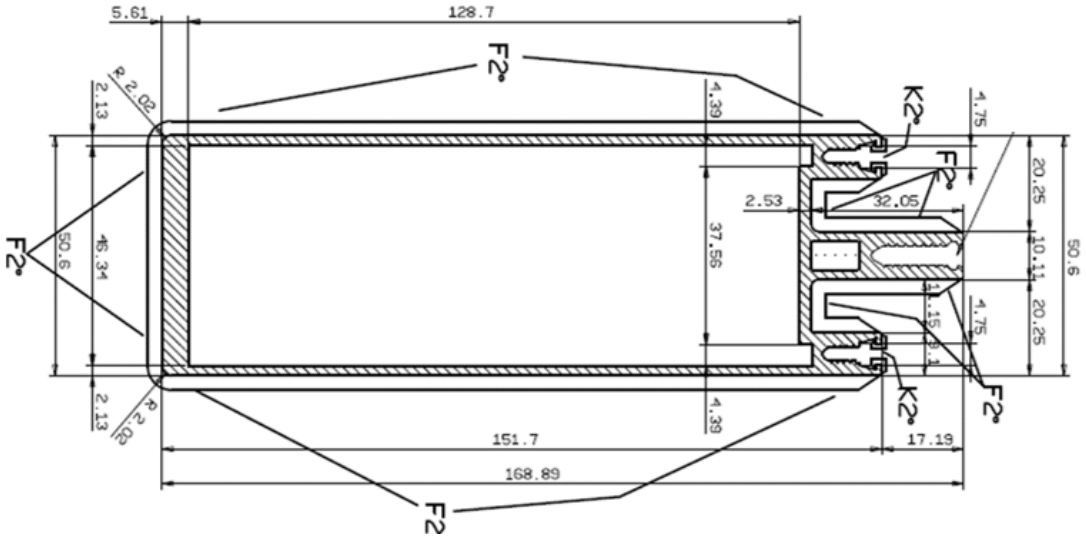

Fig. 2. Geometry of the extruded profile.

In Table 1, the extrusion process and the geometry parameters of billet and tools are reported.

Table 1. Process parameters and geometry tolerances.

Process parameters and geometry tolerances	**Profile**
Aluminum alloy	AA6060
Extrusion ratio	27
Ram speed [mm/s]	8
Container temperature [°C]	430
Billet temperature [°C]	480
Die temperature [°C]	510
Ram acceleration time [s]	5
Billet length [mm]	950
Billet diameter [mm]	203
Container diameter [mm]	211
Billet Rest length [mm]	44

The microstructure of the profile is reported in Fig. 3b-g. The investigated samples were grinded, polished and etched with electrolytical etching. The images of the etched samples were acquired by using polarized light microscopy Zeiss AXIO and the measurement of the average grain dimension was carried out according to the ASTM-E112 regulation. The images of Fig. 3 clearly show a fully recrystallized microstructure, within an average dimension range of 45 μm to 110 μm. The analysed samples were taken at the middle length of the extrusion profile, corresponding to a ram stroke of 475 mm. From the entire cross-section of the profile, six zones were selected (Fig. 3b-g). From each zone, 10 random points were extracted and, in each of these, the dimensions of the statically recrystallized diameter were measured. Half of these grain sizes were used for the model calibration and the other half for the validation. During the calibration, these values were used to find the material constants of the recrystallization model while, during the validation, the values were used to assess the accuracy of the model predictions.

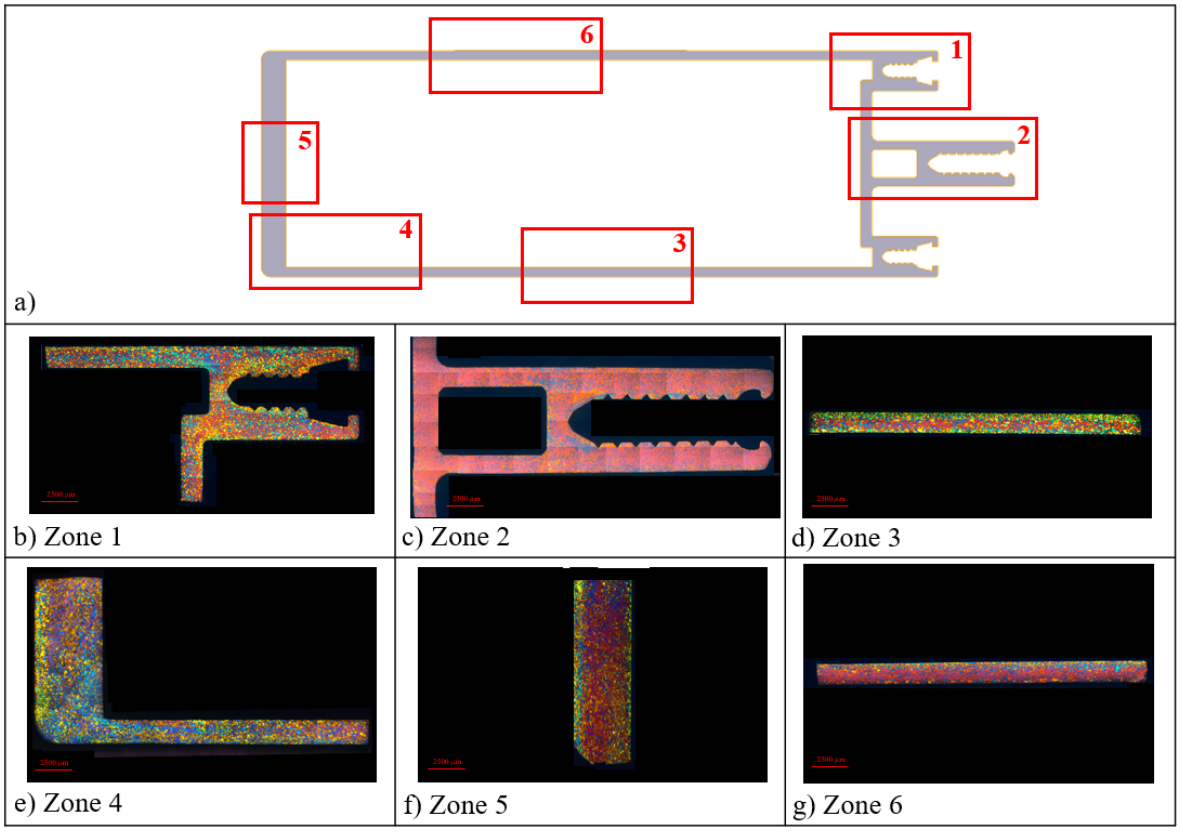

Fig. 3. Microstructure of the investigated AA6060 profile.

Modeling

The static recrystallization kinetic was modeled according to [8]: the average diameter of the static recrystallized grain D_{rex} was calculated as following:

$$D_{rex} = X_{rex} * N^{-1/3} \quad (1)$$

where N is the nucleation density and X_{rex} is the fraction of recrystallized material. The X_{rex} value was considered equal to 1 since the acquired images show a completely recrystallized microstructure. In order to determine N, different nucleation contributions must be considered [8]:

$$N = N_{PSN} + N_{GB} + N_C \quad (2)$$

where N_{PSN} is the nucleation occurred from deformation zones around particles larger than a critical size. It is often the main nucleation mechanism in 6XXX aluminum alloys which contains large undeformable particles, and involves the growth of nuclei in turbulent deformation zones with random orientations. N_{GB} is the nucleation from old grain boundaries and N_C is the nucleation from retained cube grains which survived the applied deformation. These three contributions can be calculated as following [8]:

$$N_{PSN} = C_{PSN}\, exp\left(\frac{-A_{PSN}}{(Pd-Pz)}\right) \quad (3)$$

$$N_{GB} = C_{GB}\, \delta\, A(\varepsilon)\, S_{GB} \quad (4)$$

$$N_C = C_C\, \delta\, A(\varepsilon)\, S_C \quad (5)$$

where C_{PSN}, A_{PSN}, C_{GB} and C_C are the material constants which need to be calculated in order to optimize the model for the investigated AA6060 aluminum alloy. Pd is the Stored Energy, driving force for recrystallization which act in the form of dislocation substructures and concentrations of vacancies [9]. Pz is the Zener Drag Pressure, retarding force for recrystallization which depends on the dispersoids size and density and alloying elements in solid solution [10].

$$Pd = \frac{Gb^2}{10}\left[\rho i(1 - ln(10b\rho i^{0,5})) + \frac{2\theta}{b\delta} * \left(1 + ln\ ln\ \left(\frac{\theta c}{\theta}\right)\right)\right] \quad (6)$$

where G is the material shear modulus (2.05x10^{10} Pa), b the Burgers vector (2.86x10^{-10} m), ρi the dislocation density, δ the subgrain size, θ the misorientation angle and Θc the misorientation angle limit (15°). The dislocation density ρi and the misorientation angle θ were calculated according to [9] as a function of the strain rate $\dot{\varepsilon}$, the temperature T and the strain ε (Fig. 4a,b).

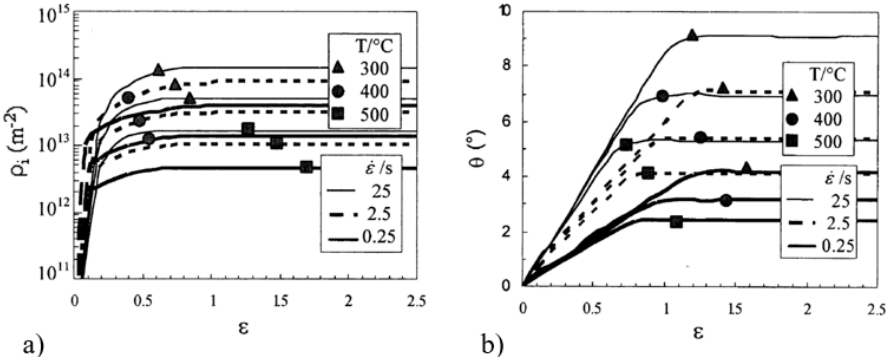

Fig. 4. a) Dislocation density [9], b) Misorientation angle [9].

The subgrain size and the Zener-Hollomon parameter were calculated according to [11]:

$$\frac{1}{\delta} = C\ (lnZ)^n \quad (7)$$

$$Z = \dot{\varepsilon}\ exp\ \left(\frac{Q}{RT}\right) \quad (8)$$

where C=3.36x10^{-9} m^{-1}, n=5.577, Q is the activation energy of the AA6060 (161000 J/mol*K [12]), R is the universal gas constant (8.341 J/mol) and $\dot{\varepsilon}$ is the maximum strain rate for each point of material flow during the extrusion deformation path.
$A(\varepsilon)$ is the grain boundary area per volume at a given strain and S_{GB}, which can be assumed as S_{GB}=S_C=S [13], is the number of subgrain larger than a critical subgrain size δ^*, calculated as followed:

$$\delta^* = \frac{4\gamma}{Pd - Pz} \quad (9)$$

According to what reported in literature [8], $A(\varepsilon)$ was modelled as:

$$A(\varepsilon) = \frac{1}{D_0}[(exp\ exp\ (\varepsilon)\ + exp\ exp\ (-\varepsilon)\ + 1)] \quad (10)$$

where D_0 represents the average grain size in the billet material after the homogenization process. According to the work of [10], the Zener Drag pressure is calculated as following:

$$Pz = \frac{3 * f * \gamma}{4 * r} \quad (11)$$

where f and r are the fraction area and the mean size of the dispersoids, respectively, and γ is the grain boundary energy (0.3 J/m^2 [13]). As an approximation, values of f and r were taken from the work of [14], where the distribution of dispersoids were analysed in different AA6060 aluminum alloys (f= 0.013%, r= 125 nm).

Numerical Investigation

The simulation of the analysed extrusion process was performed using Qform Extrusion, a commercial ALE (Arbitrarian Lagrangian Eulerian) FE code. The constitutive model used for the description of the AA6060 flow stress was proposed by Hensel-Spittel [15]. According to the proposed equation (Eq. 12), the material flow stress $\underline{\sigma}$ depends on the contribution of strain $\underline{\varepsilon}$, strain rate $\underline{\dot{\varepsilon}}$ and temperature T:

$$\underline{\sigma} = A \cdot e^{m_1 T} \cdot \underline{\varepsilon}^{-m_2} \cdot \underline{\dot{\varepsilon}}^{-m_3} \cdot e^{\frac{m_4}{\underline{\varepsilon}}} \cdot (1+\underline{\varepsilon})^{m_5 T} \cdot e^{m_7 \underline{\varepsilon}} \cdot \underline{\dot{\varepsilon}}^{m_8 T} \cdot T^{m_9} \quad (12)$$

The values of the Hensel-Spittel constants ($m1$-$m9$) used for the simulation of the AA6060 aluminum alloy, reported in Table 2, were taken from the Qform material database.

Table 2. Hensel-Spittel and for the AA6060 aluminum alloy.

Parameters	AA6060
A	280 [MPa]
m1	-0.00461 [K^{-1}]
m2	-0.16636
m3	0.12
m4	-0.02056
m5	0.00036 [K^{-1}]
m7	0
m8	0 [K^{-1}]
m9	0

The friction conditions between workpiece and tools were also taken from the software database according to the default values optimized for extrusion (Table 3). The values of the material properties used in the simulation are reported in Table 4.

Table 3. Friction conditions.

Surface	Friction condition
Billet-Container	Sticking condition
Billet-Ram	Sticking condition
Billet-Die	Sticking condition
Bearings	Levanov model (m = 0.3, n = 1.25)

Table 4. Material parameters for the AA6060 aluminum alloy.

Material Properties	AA6060
Density [Kg/m3]	2690
Specific heat [J/kg K]	900
Thermal conductivity [W/m K]	200
Thermal expansivity [m/K]	2.34*10-5
Young's modulus [GPa]	68.9
Poisson's ratio	0.33

In order to validate the results of the simulation, the values of the numerical extrusion load and profile exit temperature were compared to the experimental ones. With regard to the extrusion load, the experimental peak value was found at 23.4 MN while the numerical one at 23.3 MN. Consequently, the numerical error in the extrusion load prediction was under the 1%. Moreover, the experimental exit temperature of the profile (recorded by using a pyrometer fixed at the exit of the die) was found at 557°C while the numerical one at 562°C, with a prediction error close to the 1%. As a result, the average error in the extrusion load and temperature prediction was found below the 1%, thus proving the reliability of the simulation.

Results and Discussion

The material constants of the recrystallization model were obtained by applying the Levenberg-Marquardt non-linear regression algorithm [16], implemented in Matlab®, using as input data the "calibration set" of points in which the grain size was experimentally calculated. For each considered point, the values of temperature, strain and maximum strain rate were calculated by the simulation using Qform software. A different set of points ("validation set") were used to validate the results of the numerical microstructure prediction.

Considering the trend of eq. 10, since this equation was investigated in rolling processes which typically have stain values considerably lower than 10 [8], it has been noticed that for values of strain higher than 10 (Fig. 5a), typical of industrial-scale extrusions, the formula returned unreasonably high values of $A(\varepsilon)$ and, consequently, of N_{GB} and N. For this reason, $A(\varepsilon)$ has been calculated according to eq. 13, limiting the growth of the parameter to a maximum value (Fig. 5b):

$$A(\varepsilon) = \frac{1}{D_0}\left[p_1 - p_2\, e^{p_3\, \varepsilon^{p_4}}\right] \tag{13}$$

where p_1, p_2, p_3, p_4 are material constants. These values were added to the other material constants and optimized using the Levenberg-Marquardt algorithm mentioned above.

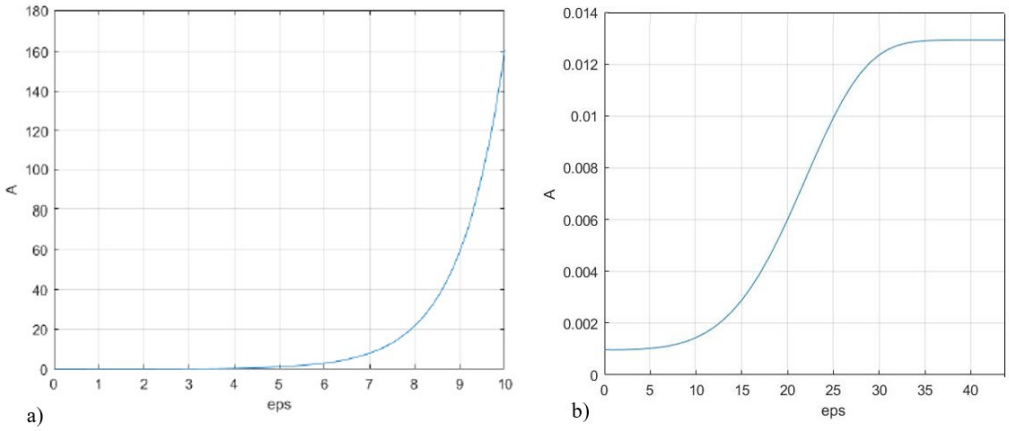

Fig. 5. a) A(ε) calculated according to Eq. (10), b) schematization of A(ε) calculated according to Eq. 13.

The outputs of the non-linear regression method are summarized in Tab. 5. After acquired these values, the model was implemented into Qform Extrusion and used to calculate the average grain size of the extruded profile.

In Fig. 6, the numerical simulation of the grain size after the complete SRX is reported. Red and blue areas correspond to the part of the profile in which the grain size have higher and lower dimensions, respectively. The numerical range of grain size dimension resulted between 52 μm and 96 μm.

Table 5. Recrystallization model material constants AA6060.

Material constants	**AA6060**
C_{PSN}	5.00021 e^{13}
A_{PSN}	872954
C_{GB}	0.0002145
C_C	0.0002145
p_1	1.9
p_2	1.06
p_3	1 e^{-7}
p_4	6

Fig. 6. Numerical average grain size of the investigated extruded profile.

In Fig. 7, the comparison between experimental and numerical grain size calculated in the "validation set" of points is reported. In details, the x-axis represents the diameter of grains experimentally measured while the y-axis represents the numerical predicted dimensions. Consequently, if the numerical measure perfectly matches the experimental one, the point is expected to be exactly on the 45° green line.

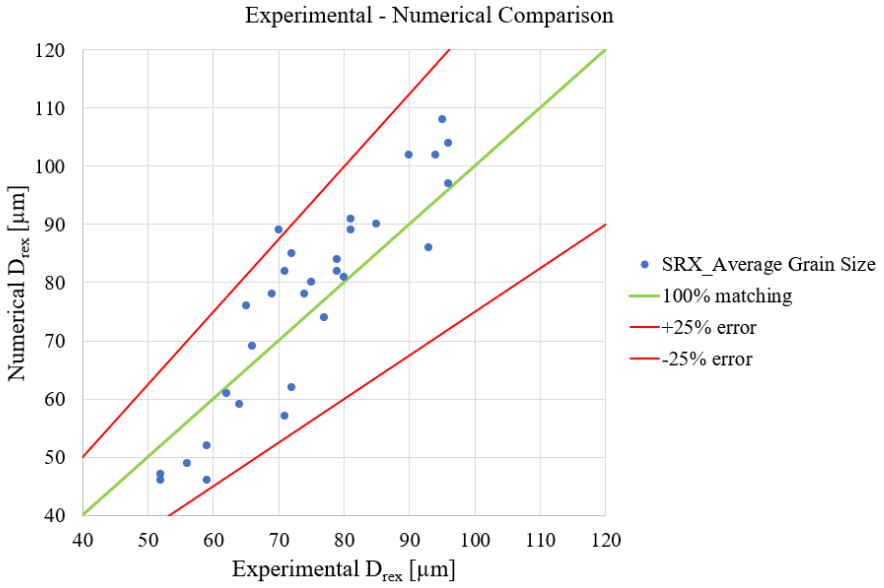

Fig. 7. Comparison between experimental and numerical grain size.

In order to facilitate the understanding of the prediction accuracy, two additional red lines were reported corresponding to a ± 25% of error. Since the high number of both process and

metallurgical factors affecting the final grain size, the industrial complexity of the analysed extruded geometries and the approximations deriving from the selected measurement methodology for the experimental analysis of the grain dimension, the range of ± 25% of error, also used by Donati L. et al. in [11] for the analysis of a laboratory-scale extruded profile, should be considered as a range of excellent prediction accuracy. As can be seen in Fig. 10, over the 95% of the blue dots fall within the red lines, thus proving the accuracy of the developed recrystallization model.

Summary

In the present work, the development of the recrystallization model of the AA6060 aluminum alloy was carried out together with the FE simulation using Qform Extrusion code. The microstructural analysis of the profile was performed and the collected data were used for the validation of the proposed model. The main outcomes of this work can be summarized as following:

- An innovative static recrystallization model was developed and optimized using the data experimentally acquired from the investigate AA6060 extruded profile.
- The prediction error of the average grain size in over the 95% of the analysed points remain below the ± 25% thus proving the good experimental-numerical agreement and the reliability of the proposed model. Further investigations are still needed to investigate the model accuracy in different AA6060 extruded profiles.

References

[1] L. Donati, B. Reggiani, R. Pelaccia, M. Negozio, S. Di Donato, Advancements in extrusion and drawing: a review of the contributes by the ESAFORM community, Int. J. Mater. Form. 15 (2022). https://doi.org/10.1007/s12289-022-01664-w

[2] C. Zhang, C. Wang, Q. Zhang, G. Zhao, G.L. Chen, Influence of extrusion parameters on microstructure, texture, and second-phase particles in an Al-Mg-Si alloy, J. Mater. Process. Technol. 270 (2019) 323-334. https://doi.org/10.1016/j.jmatprotec.2019.03.014

[3] C. Zhang, C. Wang, R. Guo, G. Zhao, L. Chen, W. Sun, X. Wang, Investigation of dynamic recrystallization and modeling of microstructure evolution of an Al-Mg-Si aluminum alloy during high-temperature deformation, J. Alloy. Compd. 773 (2018) 59-70. https://doi.org/10.1016/j.jallcom.2018.09.263

[4] T. Zhang, L. Li, S. Lu, L. Zhengfang, P. Chen, G. Hai, Static recrystallization kinetics and microstructure evolution of 7055 aluminum alloy, Metall. Res. Technol. 116 (2019) 120. https://doi.org/10.1051/metal/2018046

[5] T. Furu, R. Østhus, N. Telioui, R. Aagård, M. Bru, O.R. Myhr, Modeling the Effect of Mn on Extrudability, Mechanical Properties and Grain Structure of AA6082 Alloys, Proceedings of the Eleventh International Aluminum Extrusion Technology Seminar ET 2016, Chicago 3-6, 1 (2016) 567-590.

[6] A.R. Eivani, H.R. Jafarian, J. Zhou, Simulation of peripheral coarse grain structure during hot extrusion of AA7020 aluminum alloy, J. Manuf. Process. 57 (2020) 881-892. https://doi.org/10.1016/j.jmapro.2020.07.011

[7] Z. Peng, T. Sheppard, Prediction of Static Recrystallisation after Extrusion of Shaped Aluminium Sections, Mater. Sci. Forum 467–470 (2004) 407-420. https://doi.org/10.4028/www.scientific.net/msf.467-470.407.

[8] H.E. Vatne, T. Furu, R. Orsund, E. Nes, Modelling recrystallization after hot deformation of aluminum, Acta Mater. 11 (1996) 4463-4473. https://doi.org/10.1016/1359-6454(96)00078-X

[9] C.M. Sellars, Q. Zhu, Microstructural modelling of aluminium alloys during thermomechanical processing, Mater. Sci. Eng. A 280 (2000) 1-7. https://doi.org/10.1016/S0921-5093(99)00648-6

[10] F.J. Humphreys, M. Hatherly, Recrystallization and related annealing phenomena, Second edition, Elsevier, Oxford, UK, 2004.

[11] L. Donati, A. Segatori, M. El Mehtedi, L. Tomesani, Grain evolution analysis and experimental validation in the extrusion of 6XXX alloys by use of a lagrangian FE code, Int. J. Plast. 46 (2013) 70-81. https://doi.org/10.1016/j.ijplas.2012.11.008
[12] M. Cheng, Effect of preheating condition on strength of AA6060 Aluminium Alloy for extrusion. Diss. Auckland University of Technology, 2010.
[13] C.O. Paulsen, Recrystallization Behaviour in Extruded Profile of Non-Dispersoid Containing Al-Mg-Si Alloys, PhD Thesis, Department of Materials Science and Engineering NTNU-Trondheim, Materials Science and Engineering, 2015.
[14] Q. Xiaoming, N. Parson, X. Grant Chen, Effect of post-homogenisation cooling rate and Mn addition on Mg2Si precipitation and hot workability of AA6060 alloys, Canadian Metallurgical Quarterly 59 (2020) 189-200. https://doi.org/10.1080/00084433.2020.1719332
[15] A. Hensel, T. Spittel, Kraft und Arbeitsbedarf bildsamer Formgeburgsverfahren, 1. Auflage, Leipzig: VEB Deutscher Verlag fur Grundstoffindustrie, 1978.
[16] P.E. Gill, W. Murray, Algorithms for the Solution of the Nonlinear Least-Squares Problem, SIAM J. Numeric. Analys. 15 (1978) 977-992. https://doi.org/10.1137/0715063